

Ink-Particle Simulation for Continuous Inkjet Type Printer

Masato Ikegawa¹, Masanori Ishikawa¹, Eiji Ishii¹, Nobuhiro Harada² and Tsuneaki Takagishi²

¹Center for Technology Innovation-Mechanical Engineering, Hitachi Ltd., Ibaraki, Japan

²Marking Systems and Hoist Systems Division, Hitachi Industrial Equipment Systems Co., Ltd., Ibaraki, Japan

Abstract

Industrial continuous inkjet printers are typically used for printing directly onto various types of products such as cans, bottles, and food packaging in production lines. To enable their application to higher speed production lines, their print quality needs to be improved. This means that ink-particle simulation technology is needed to clarify the factors that affect print quality. Print distortion is caused by certain droplet shapes in inkjet breakup and aerodynamic and electric interference among the ink particles flying from the nozzle to the print target. A simulation technique has been developed that enables the breakup into droplets and the trajectories of the ink particles flying from the nozzle to the print target to be calculated with initial data obtained by breakup simulation. Printing of a line of seven dots was simulated well with this simulation code without initial particle input data. Also print distortion was prevented by inserting dummy particles between charged ones in the simulation.

Introduction

Since continuous inkjet printers (CIJPs) were originally devised by several inventors, e.g., Thomson [1], Sweet [2], and Herz and Simonsson [3], they have been improved for practical uses. Industrial CIJPs are used on many production lines for printing on various types of products such as cans, bottles, and food packaging [4, 5] because the maximum print distance is set greater and the maximum printing speed is higher than those of drop-on-demand printers.

However, the print quality now needs to be improved for use in higher speed production lines. Therefore, ink-particle simulation for formation and flight is needed to clarify the factors that affect print distortion.

The ink particles in CIJPs are formed by the breakup of the liquid jet ejected from the nozzle, charged between the charging electrodes, deflected by the deflection electrodes, and then they reach the print target. Print distortion is caused by the certain droplet shapes as a result of the inkjet breakup and aerodynamic and electric interference among the ink particles flying from the nozzle to the print target. The breakup into droplets, trajectories of the ink-particles flying from the nozzle to the print target and airflow caused by them is calculated in the simulation.

The mechanism for droplet formation in CIJPs was theoretically investigated by Rayleigh [6], Weber [7], and Tomochika [8], and it was recently simulated with a computer [9, 10]. The mechanism for droplet charging and deflection was investigated by Suzuki and Asano [11] and Filmore et al. [12]. Droplet spreading on the target was investigated by Ikegawa and Azuma [13].

We have also developed an ink-particles' flight simulation [14, 15], but it needs the diameter, initial velocity, and initial interval of

particles as input data, which has to be measured by high speed camera.

In this study, we have developed a simulation of the inkjet breakup into droplets and the trajectories of the ink particles flying from the nozzle to the print target by connecting the inkjet breakup simulation and ink-particle flight simulation with ink-particle data.

Numerical Simulation

Problem Phenomena

Figure 1 is a schematic of the principles underlying a CIJP. An ink-supply pump (not shown) pressurizes the ink so that it flows through the nozzle. Ultrasonic vibration breaks the pressurized ink stream into small droplets. The droplets then fly sequentially with a certain interval from the nozzle toward the print target. Each droplet is selectively charged by charge electrodes that apply a signal that corresponds to the character to be printed. A high voltage is applied to the deflection electrodes. As the charged droplets pass between these electrodes, they are deflected by an amount proportional to the charge. The charged droplets then reach the print target, which they hit sequentially from bottom to top. The target moves across the print head almost at right angles to the direction of the deflected droplets. In this manner, printed characters are formed as two-dimensional dot matrices on the target. The non-charged droplets that are not used for printing are caught by a gutter and returned as ink to an ink bottle (not shown). The droplets are called "ink particles" here. An airflow is induced around them during flight. Print distortion occurs due to small particles (satellite) formed during the inkjet breakup and changes in their flight trajectories resulting from aerodynamic and Coulomb interference between them.

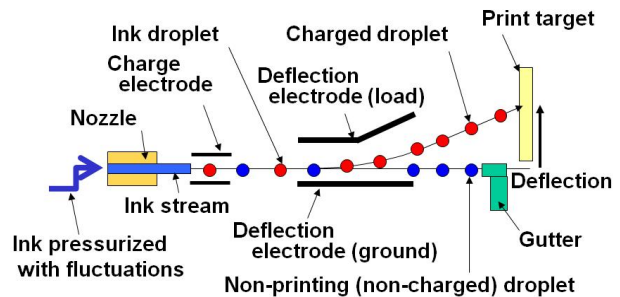


Figure 1 Schematic of principles for continuous inkjet printer

Numerical analysis

The numerical analysis was done using three-dimensional fluid simulations with incompressible and isothermal conditions and the finite volume method under a conservative scheme was used. The governing equations, i.e., a continuity equation and the Navier-

Stokes equation, are written as

$$\begin{cases} U_{i,i} = 0 \\ \dot{U}_i = -P_j / \rho + \nu(U_{i,j} + U_{j,i})_j \end{cases}, \quad (1)$$

where U_i is the i th component of velocity, $U_{i,j}$ is the x_j directional derivative of U_i , and \dot{U} is the time derivative of U . Here, P_j is the x_j directional derivative of pressure P , ρ is the density, and ν is the kinematic viscosity. The subscripts used comply with the summation law.

Almost 260 ink-particles were needed to predict the printed characters in the simulation. It was impractical to build fine meshes around 260 ink particles and analyze them as an Eulerian two-phase flow due to the massive amount of calculations that would be needed. Therefore, we devised a simulation technique where the breakup simulation and flight simulation were divided, and the trajectories of the ink-particles flying from the nozzle to the print target were calculated with initial data obtained by the breakup simulation.

1) Inkjet breakup simulation

The breakup into droplets was simulated by solving the two-phase flow of the 3D-Navier-Stokes equation with the VOF (volume of fluid) method. The VOF method used in this study was for simulating the free surface flow. The volume fraction of liquid on each computational mesh was defined as α .

$$\frac{\partial \alpha}{\partial t} + \bar{u} \nabla \alpha = 0 \quad (3)$$

The density ρ in Eq. 2 was modified to

$$\rho = \rho_{liquid} \alpha + \rho_{gas} (1 - \alpha) \quad (4)$$

where ρ_{liquid} is the density of the liquid and ρ_{gas} is the density of the gas. The viscosity μ in Eq. 2 was modified to

$$\mu = \mu_{liquid} \alpha + \mu_{gas} (1 - \alpha) \quad (5)$$

where μ_{liquid} is the density of the liquid and μ_{gas} is the density of the gas.

The continuum surface force (CSF) model was used for calculating the surface tension force. The pressure drop Δp across the surface is defined as

$$\Delta p = \sigma \kappa \quad (6)$$

where σ is the surface tension and κ is the surface curvature.

The surface curvature defined by the CSF model is calculated as

$$\kappa = -\nabla \cdot \left(\frac{\nabla \alpha}{|\nabla \alpha|} \right) \quad (7)$$

The surface tension force f_{sf} is defined as

$$f_{sf} = \sigma \kappa \frac{\nabla \rho}{\rho_{liquid} - \rho_{gas}} \quad (8)$$

Figure 2 shows a simulation model for a continuous inkjet nozzle, and Figure 2(b) is an enlarged view of around the nozzle. Figure 2(a) is an entire view of the simulation model including the inkjet nozzle and air region. Theoretically, the asymmetric disturbance was stable : only the axisymmetric disturbance was unstable and broke up the liquid pillar into droplets [6]. Therefore, a two-dimensional axisymmetric model was used. The left side of the model was the inlet boundary, and the top and right side of the

air region were the pressure boundaries. The bottom of the model was the center axis. The other boundaries were wall boundaries with non-slip wall condition. The nozzle was a cylindrical straight pipe with diameter d (0.065 mm) and length L ($= L/d = 0.85$). The air region was $154d \times 4.6d$. The diameter of the inlet was $12.3d$, and the ink went through the ink room at a velocity of U_0 . The ink went out to the air region through the nozzle.

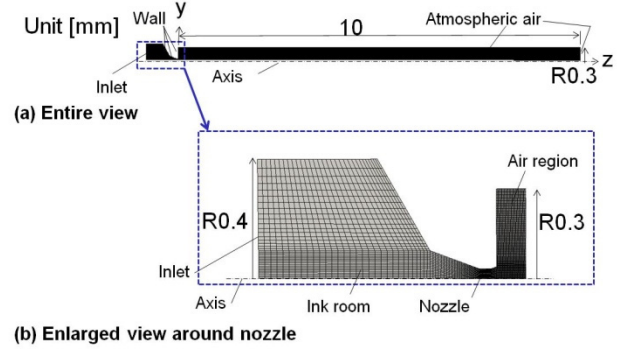


Figure 2 Simulation model and mesh for inkjet breakup simulation

The inlet velocity $U(t)$ was defined as

$$U = U_0 (1 + C * \cos(2\pi f t)) \quad (9)$$

where C is the amplitude of disturbance, f is the piezo frequency, and t is the time. The fluctuation range of the inlet velocity depended on the amplitude C , and this fluctuation caused a disturbance on the surface of the liquid column.

Table 1 lists the material properties; the densities of the ink and air were 890 kg/m^3 and 1.21 kg/m^3 , respectively, and their viscosities were $25.4 \times 10^{-3} \text{ Pa}\cdot\text{s}$ and $1.85 \times 10^{-5} \text{ Pa}\cdot\text{s}$, respectively.

Table 1 Material properties of fluids

Liquid (Ink)	Density ρ [kg/m^3]	890
	Viscosity μ [$\text{Pa}\cdot\text{s}$]	2.9×10^{-3}
	Surface tension [N/m]	25.4×10^{-3}
Gas (Air)	Density ρ [kg/m^3]	1.21
	Viscosity μ [$\text{Pa}\cdot\text{s}$]	1.85×10^{-5}

The interFoam solver (OpenFOAM v2.1.1) [16] was used in the inkjet breakup simulation. The number of computational meshes was 294,098. We used a space and time differential scheme using second order and first order accuracies, respectively. The time step was automatically controlled so that the local courant number defined at each mesh was set to less than 0.5.

The breakup length of the liquid column was affected by the prediction accuracy of the capillary waves on the surface of the liquid column, so it was important to use a sufficiently accurate scheme for the inkjet breakup simulation. We evaluated the effect of two convection schemes, the first order accuracy and second order accuracy schemes and selected the last one on the liquid

column breakup length. An amplitude C of 0.1 was used in this case.

From this simulation, the diameter, initial velocity, and initial interval of particles were obtained.

2) Ink-particle flight simulation

The details of the method of the ink particle flight simulation have been reported [14]. Here the summary is explained. The necessary functions, such as calculating the electrostatic force, Coulomb force, and aerodynamic drag force were added to a Lagrangian method for fluid dynamic analysis. The airflow and electric field were calculated using STAR-CD computational fluid dynamics software (v.4.10) [17].

A dispersed multi-phase flow model (Lagrangian model) was better for analyzing the flow as the dispersed phase of a continuous aspect of the vapor phase and the particles, and the trajectories of the ink particles were calculated as kinetics with outside forces while the airflow was analyzed under unsteady conditions. Unsteady flow was calculated by using the pressure implicit with unstaying of operator (PISO) method with a fully implicit method.

The outside forces that affect an ink particle are Coulomb force F_{cl} from other charged ink particles, air drag F_{dr} from the surrounding air, and electric force F_{el} from the static electric field. In addition, small particles are generally subject to gravity, virtual mass force, and Basset force, but these effects were neglected here because they were very small under our simulation conditions.

Newton's equation of motion for a particle is

$$m_d \frac{dU_d}{dt} = F_{dr} + F_{el} + F_{cl} \quad (10)$$

where m_d is the mass of the particle, U_d is its velocity, and t is the time.

Equation (10) was integrated with the first order of Euler's implicit method, and the momentum changes exchanged through the transported fluid in the cell through which the particle passes in the dispersed multi-phase flow (Lagrange model) method. The conversion rate of the entire mass and energy was similarly evaluated through integration and the sum total of the corresponding equation.

Air drag F_{dr} can be written as follows using drag coefficient C_D :

$$F_{dr} = \frac{1}{2} C_D \rho A_d |U - U_d| (U - U_d) \quad (11)$$

where ρ is the density of air, A_d is the sectional area of the ink-particle, and U is the velocity of the surrounding air.

Ink particles were assumed to be spherical on the basis of measurements obtained from a photograph taken after such particles passed between the deflection electrodes. We used Beard and Pruppacher's empirical equation below for C_D [18].

$$\begin{aligned} C_D &= (24 / Re_d)(1 + 0.102 Re_d^{0.955}) & (0.2 < Re_d < 2) \\ C_D &= (24 / Re_d)(1 + 0.115 Re_d^{0.802}) & (2 < Re_d < 21) \\ C_D &= (24 / Re_d)(1 + 0.189 Re_d^{0.632}) & (21 < Re_d < 200) \end{aligned} \quad (12)$$

where Re_d is the particle Reynolds number, which is defined as

$$Re_d = \frac{|U - U_d| d_d}{\nu} \quad (13)$$

where ν is the kinematic viscosity of air.

What needs special attention here depends on the expressions in Eqs. (11) and (12); F_{dr} is a function at the relative speed $(U - U_d)$,

and U in the surrounding airflow has an important effect. Lined ink particles drew peripheral air into the stream, thus generating a jet boundary layer, which greatly increases the velocity of the surrounding airflow.

Several groups have examined experimentally the drag coefficient of a trailing sphere [14]. Tsuji et al. plotted the relationship of the drag coefficient ratio between a trailing sphere and a single sphere, C_D/C_{D0} , and interval L between the two spheres in a tandem arrangement [19]. The drag coefficient, C_D , of the trailing sphere decreased more than that of a single sphere, C_{D0} when the $L/\text{diameter } D_{sp}$ ratio was less than six. The empirical formula fitted with a second order approximation for Tsuji et al.'s experimental data was used in the subroutine to calculate drag in the simulation of flying ink particles. Tsuji et al. also found that the drag coefficient of the leading sphere was unaffected by the trailing sphere.

The static electric field was analyzed with the STAR-CD software. Electric force F_{el} in Eq. 10 was applied to an ink particle with charge q in electric field E between the deflection electrodes.

$$F_{el} = qE \quad (14)$$

The Coulomb force F_{cl} on an ink particle is the sum of the Coulomb forces from all the other ink particles surrounding it. Therefore, all the ink particles surrounding the ink particle under examination (with charge q) were identified, and the Coulomb forces from all the ink particles at distance r_i and with charge q_i are summed up :

$$F_{cl} = \sum \frac{1}{4\pi\epsilon_0} \frac{qq_i}{r_i^2} \quad (15)$$

where $\epsilon_0 = 8.854E-12$ [$A^2s^2N^{-1}m^{-2}$] is the permittivity of the vacuum electric constant.

The calculation area is the space from the inlet (nozzle exit) to the print target, as illustrated in Fig. 3. The ink particles flew along the yz plane. The area for the calculations was enclosed by the charge electrodes, deflection electrodes, print target, and atmospheric pressure boundaries. The direction of x was established to be 1.6 mm in width and symmetry boundaries were created for both walls.

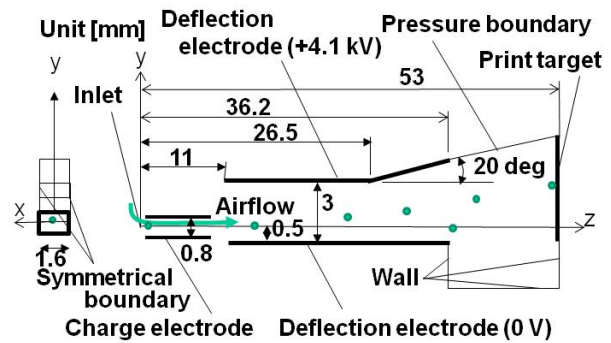


Figure 3 Simulation model for ink particle flight simulation

The ink particles were sequentially discharged from the starting point (middle of charge electrode, $x = y = 0$, $z = 5$ mm) in the z direction at an initial speed and constant interval. They form an "ink beam", that passed along the center line between the charge electrodes and along a line 0.5 mm above the ground deflection electrode. The gutter into which non-charged ink particles entered

was neglected in the simulation. The voltage of the positive deflection electrode was set to +4.1 kV, and that of the ground deflection electrode was set to 0 V.

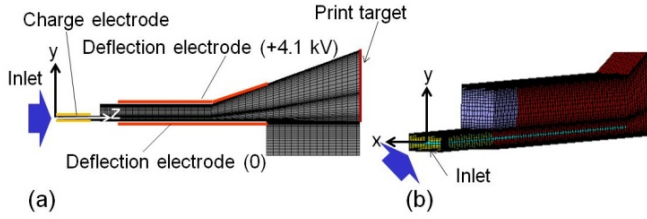


Figure 4 (a) Entire mesh chart (202,548 cells), and (b) mesh chart as viewed from inlet for ink particle flight simulation

The mesh (hexahedron) used for the STAR-CD analysis (shown in Fig. 4) had 202,548 cells. The first-order central difference method was used for calculating the space derivatives.

Since the Reynolds numbers for the airflow and the ink particles were ~400 and ~200, respectively the flow could be treated as a laminar flow. Therefore an unsteady airflow, laminar airflow, and two-phase flow (Lagrangian) were used.

The simulation code was verified by the experimental results for the change in velocities and trajectories for two flying ink particles with a certain interval. The simulated aerodynamic effects were first verified by the velocities of two non-charged ink particles, and then the simulated aerodynamic and electrical effects were verified by the trajectories of two charged ink particles flying between the deflection electrodes [14]. Since many more particles than two fly toward the print target, we investigated the effect of interferences among many particles on print quality here.

We investigated the printing of one line with seven dots. Table 2 shows the ink-particle charges for seven dots.

Table 2 Ink-particle charges of seven dots

Dot no.	Charge [C]
1	-7.735×10^{-13}
2	-9.203×10^{-13}
3	-1.067×10^{-12}
4	-1.213×10^{-12}
5	-1.361×10^{-12}
6	-1.508×10^{-12}
7	-1.655×10^{-12}

Results and Discussion

The inkjet breakup simulation was performed, and the ink-particle flight simulation was executed by using the output data of the inkjet breakup simulation.

Inkjet breakup simulation

The result of the breakup into droplets for $C = 0.100$, $f = 68.9$ kHz, $U_0 = 0.139$ m/s are shown in Fig. 5. The disturbance of the liquid surface grew in the z-direction and caused breakup into droplets. The breakup length z_b was 4.4 mm.

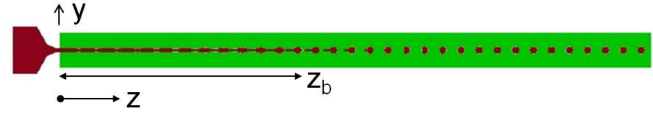


Figure 5 Simulation results of breakup into droplets by inkjet breakup simulation

From this simulation, the diameter, initial velocity, and interval of particles were obtained as shown in Table 3.

Table 3 Results of ink particles at $z = 5.0$ mm after breakup of inkjet

Initial ink-particle velocity w_{d0} [m/s]	21.0
Diameter of ink-particle d_d [μm]	112
Initial interval L_0 [μm]	300

From the input data of diameter, initial velocity, and initial interval of particles, ink-particle flight simulation was executed.

Ink particle flight simulation

The results of the electric potential and electric field distribution in the computed model are shown in Fig. 6. The electric field was uniform between the parallel part of the deflection electrodes and decreased more than 50% in the part where the upper electrode was diagonal.

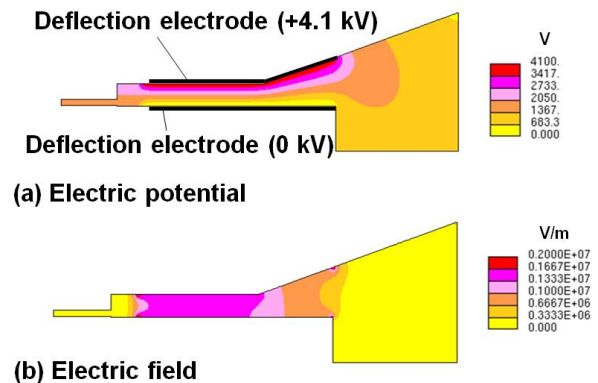


Figure 6 Simulated electric potential and electric field distribution (deflection-electrode voltage 4.1 kV)

In the simulation, the charged particles for forming one line with seven dots flew after 200 non-charged particles had flown. The particles were sequentially discharged from the starting point

(middle of charge electrode, $x = y = 0, z = 5 \text{ mm}$) along the z axis at a constant interval. In the real printer, the non-charged particles flew continuously, and an airflow was formed before the flight of the charged particles. In the simulation, 200 non-charged particles flew first, and then the charged particles for forming one line with seven dots flew. A previous report [14] showed that the airflow distribution reached a steady state once 200 particles have flown, so the number of initial non-charged particles was set to 200.

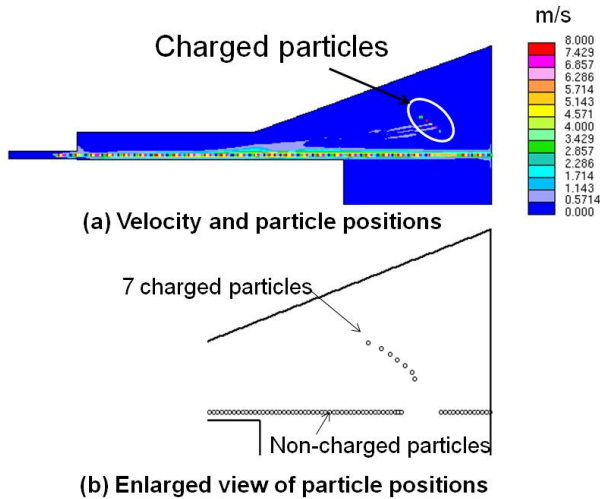
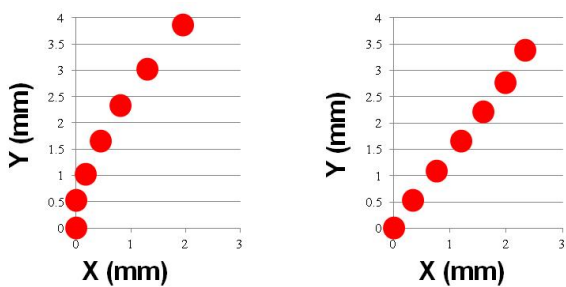


Figure 7 Velocity distribution and particle positions at 0.0020 s in ink particle flight simulation

The simulation results of the positions of the particles and the airflow velocity distribution at 0.0020 s after the first charged particle was discharged from the nozzle are shown in Fig. 7. A jet boundary layer was found to form around the flying particles. The line was found to be curved, and this caused print distortion.

Print results



(a) w/o dummy particles (b) with dummy particles

Figure 8 Print results with ink particle flight simulation

The simulation results of printing on the print target are shown in Fig. 8. The print target ran in the x direction (perpendicular to the sheet in Fig. 7) at 400 m/min. The seven particles in line are represented by the dots from bottom to top (Fig. 8(a)). The results of the particle positions revealed several print

distortions. The line was curved, and the top dots were shifted to upward and to the right. These print distortions were due to the narrower interval between charged particles. Therefore, the print distortion was corrected by increasing the interval by inserting dummy (non-charged) particles between the charged particles. Figure 8(b) shows the simulation results when inserting two dummy particles between neighboring charged particles. Print distortion was found to be corrected.

This simulation technique can thus be used to design CIJPs for decreasing print distortion in computers.

Conclusions

The formation and flight of ink particles for in an industrial continuous inkjet printer was simulated on the basis of electric and aerodynamic physics.

- 1) Droplet formation with inkjet breakup was simulated well.
- 2) The flight of charged ink particles was simulated well with parameters, i.e. diameter, initial velocity, and initial interval, obtained by inkjet breakup simulation.
- 3) The developed simulation can be used to design CIJPs with fine print quality in computers.

References

- [1] W. Thomson (Lord Kelvin), "Receiving or Recording Instruments for Electric Telegraphs," G.B. Patent 2147, 1867.
- [2] R. Sweet, "Fluid Droplet Recorder," U.S. Patent 3,596,275, 1963.
- [3] C.H. Hertz, and S.I. Simonsson, "Ink-jet Recorder," U.S. Patent 3,416,153, 1966.
- [4] S. Matsumoto, T. Inoue, J. Matsuno, and K. Sano, "Flight Stability of Droplets in an Electrostatic Ink-Jet Printer," Trans. of Japan Society of Mech. Eng. (C), 62, (596), pp.1467-1472, 1996.
- [5] M. Okano, T. Inoue, Y. Takizawa, T. Matsuda, and A. Miyao, "A New Nozzle for Continuous Inkjet Printers," J. Advanced Mech. Design, Systems, and Manuf., 4, (4), pp.764-772, 2010.
- [6] L. Rayleigh, "On the Instability of Jets," Proc. London Math. Soc. 10, pp.4-13, 1878.
- [7] C. Weber, "Zum Zerfall eines Flüssigkeitsstrahles," Z. Angew. Math. Mech. 11, pp.136-159, 1931.
- [8] S. Tomotika, "On the instability of a cylindrical thread of a viscous liquid surrounded by another viscous fluid," Proc. R. Soc, London, Ser. A., 150, pp.322-337, 1935.
- [9] S. Desai, and M. Lovell, "Computational fluid Dynamics Analysis of a Direct Write Manufacturing Process," Int. J. Nanomanufacturing, 3(3), pp.171-187, 2009.
- [10] M. Ishikawa, E. Ishii, and M. Ikegawa, "Simulation of Gas-Liquid Free Surface Flows in a Refrigerant Distributor and a Nozzle of Continuous- Inkjet," Proc. the ASME IMECE2013, No.63955, 2013.
- [11] M. Suzuki and K. Asano, "A Mathematical Model of Droplet Charging in Ink-jet Printers," J. Phys. D: Appl. Phys., Vol. 12, pp.529-537, 1979.
- [12] G.L. Filmore, W. L. Buehner, and D.L. West, "Drop Charging and Deflection in an Electrostatic Ink Jet Printer," IBM J. Res. Develop., pp.37-47, 1997.
- [13] M. Ikegawa, and H. Azuma, "Droplet Behaviors on Substrates in Thin Film Formation Using Ink-jet Printing," JSME INT. JOURNAL SERIES B; 47(3), pp. 490-496, 2004.
- [14] M. Ikegawa, E. Ishii, N. Harada, and T. Takagishi, "Development of Ink-Particle Flight Simulation for Continuous Inkjet Printer," Trans. of

ASME, J. of Manufacturing Science and Engineering, Vol. 136, No.5, No.051021, 2014.

- [15] M. Ikegawa, E. Ishii, N. Harada, and T. Takagishi, "Ink-Particle Flight Simulation for Continuous Inkjet Type Printer," Proc. of 30th International Conference on Digital Printing Technologies, pg.176, 2014.
- [16] The OpenFOAM Foundation, <http://www.openfoam.org/>
- [17] STAR-CD, CD-adapco, <http://www.cd-adapco.com>.
- [18] K.V. Beard, and H.R. Pruppacher, "A Determination of the Terminal Velocity and Drag of a Small Water Drops by Means of a Wind Tunnel," J. of the Atmospheric Sciences, 26, pp.1066-1072, 1969.
- [19] Y. Tsuji, Y. Morikawa, and K. Terashima, "Fluid-Dynamic Interaction between Two Spheres," Int. J. Multiphase Flow, 8(1), pp.71-82, 1982.

Author Biography

Masato Ikegawa received B.E. and M.E. degrees in aeronautics from Tokyo University in 1974 and 1976. In 1976, he joined Hitachi's Mechanical Engineering Research Laboratory, Japan, where he researched and developed scroll compressors, and numerical simulations for, for example, rarefied gas flow for low-pressure process reactors, LSI processes, plasmas, HDD airflows, and inkjets. He received a doctor of engineering degree from Tokyo University in 1990. Dr. Ikegawa is a fellow member of the Japan Society of Mechanical Engineers and the Japan Society of Fluid Mechanics and was on their boards of directors (2010-2011).